

Ring slot CP antenna for the hybrid electromagnetic solar energy harvesting and IoT application

Irfan Mujahidin^{1,2}, Akio Kitagawa¹

¹Microelectronic Laboratory, Department of Electrical Engineering and Computer Science, Graduate School of Natural Science and Technology, Kanazawa University, Kanazawa, Ishikawa, Japan

²Department of Telecommunication Engineering, Faculty of Electrical Engineering, Semarang State Polytechnic, Tembalang, Semarang City, Central Java, Indonesia

Article Info

Article history:

Received Nov 16, 2021

Revised Oct 26, 2022

Accepted Nov 12, 2022

Keywords:

CP antenna

Energy harvesting

Hybrid electromagnetic solar

IoT application

ABSTRACT

The research proposed a compact antenna integrated with dual-function solar cells to optimize internet of things (IoT) communication devices and energy harvesting. The use of integrated solar cells with electromagnetic elements as antennas and energy-gathering in a design is a solution for wireless communication sensors and simultaneously electromagnetic and solar energy harvesting. Radiation performance testing of solar cell antennas and optical experiments were carried out to test the ability of solar energy collection. A double feed ring slot circular polarization (CP) antenna coplanar antenna with a configuration has highly sensitive to vertical and horizontal waves. It is to accommodate the impact of circular polarization wave and solar cell distortion on antenna performance. This technology promises green communications, renewable energy, and environmental protection to combine wireless communication and green battery components. The study presents the performance and design results of a double line-feed microstrip antenna circuit connected with CP antenna on the S-band for IoT communication by accommodating electromagnetic energy transmission. The importance of adopting an integrated radio frequency (RF) solar energy harvesting strategy rather than a single source method makes this research very significant in its novelty by optimizing the analysis of multiple signal access in IoT communications.

This is an open access article under the [CC BY-SA](#) license.



Corresponding Author:

Irfan Mujahidin

Microelectronic Laboratory, Department of Electrical Engineering and Computer Science

Graduate School of Natural Science and Technology, Kanazawa University, Kanazawa, Ishikawa, Japan

Email: irfan@merl.jp

1. INTRODUCTION

Fossil energy sources are rapidly depleting, resulting in widespread pollution and the greenhouse effect. Solar energy, for example, has been used in the long term to promote sustainable energy for humans and the environment and green development. Since solar cells are essential in harvesting solar energy, it is best to combine them with other components with mutually supportive functions. Antennas combined with solar cells have received much attention in recent years for wireless communication systems. Photovoltaic power generation and wireless sensor for communication can be accomplished using the combined solar cell antenna because the film solar cell and narrowband antenna are integrated into one compact device. The film solar cell delivers inexpensive, pollution-free energy for environmental sustain, while communication can perform without a light source. Solar cell antennas are significantly more accommodating for independent and

standalone communication systems for outdoor applications benefit from self-sustaining solar energy, a compact installation area, and lower costs.

Several studies on a thin solar cell with an antenna have been published. Several patch antennas based on printed patches [1], interlocked patches [2], and transparent patches [3] have been explored using solar cells as ground. Some reflectarray designs use cross components [4], loops [5], [6], and transparent acrylic materials [7] as the basis of solar cells. By installing dielectric resonators in thin-film solar cells, the use of antennas with specialized dielectric resonators has been investigated [8], [9]. The solar cells are mounted on a stacked multi-patch to lessen the optical interference of the antenna composition and a substrate-integrated textile waveguide antenna, respectively [10], [11]. Slot and coplanar antennas are built for horizontal and vertical polarization applications using multi-band and bandgap [12], [13]. An antenna with a photovoltaic dipole [14], [15] was proposed using a solar cell as support antenna optimization. Although the above designs have achieved adequate radiation performance, solar cells are still seen as nuisance material, resulting in increased cost, mass, and complexity.

Photovoltaic integrated with coplanar and dipole antennas have been developed and published in [16], [17], directly using solar cells as the central radiator. Vivaldi antenna with ultra-wideband specification as recommended in [18] has amorphous silicon cells through cutting edge increment with gain fluctuations large enough to increase the frequency band. Broadband solar cell antennas with consistent radiation performance must simultaneously handle multiple external communication systems, such as WiFi, WiMax, and ZigBee. Although specific broadband antenna designs with adequate performance have been developed [19]-[21], their random shape makes them unsuitable for solar cell integration. The solution combines antennas and solar cells with stable performance to use a narrow band and specific new designs.

This research presents a novel circular polarized antenna based on solar cells. The dual-function small feed circuit is used for connectivity and solar energy harvesting activities for wireless internet of things (IoT). With the structure of the components in Figure 1. Figure 1 has followed forward to collect energy harvesting and combinations of electromagnetic and solar energy harvesting that is more optimal and compact than [16], [22]. New hybrid electromagnetic solar for IoT Applications and energy harvesting in Figure 1 Using a dual feed ring slot circular polarization (CP) antenna was created and studied to achieve generally consistent radiation performance. The observed impedance matching for dual charge working frequency ranges from 2.3 to 2.4 GHz, and directional radiation and gain performance for active dual applications such as communication and energy harvesting have been realized. Analyze the effects of solar cells on antenna performance and conduct optical measurements to assess the antenna's capacity to integrate optical components.

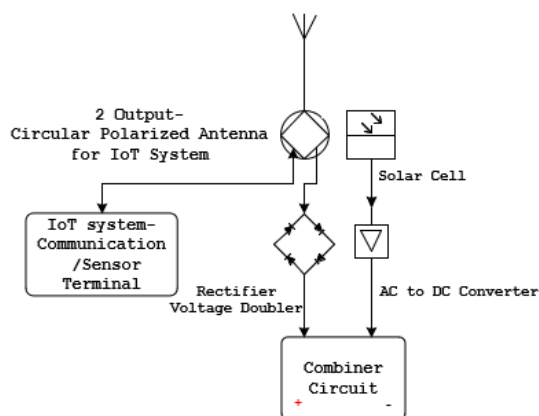


Figure 1. Schematic of hybrid electromagnetic solar energy harvesting and IoT application

2. HYBRID ELECTROMAGNETIC SOLAR-RING SLOT CP ANTENNA STRUCTURE DESIGN

The type of solar cell, namely printed thin-film organic solar cells, is used to design this dual feed ring slot CP antenna. Its 3-dimensional configuration structure is described in Figure 2. From top to bottom, the solar cell has four layers. To maintain the structure of the electromagnetic antenna, so a thin layer of organic solar cells is positioned in the sun exposure section. The alternating current (AC) energy is collected through a double feed path imprinted on the surface of the radiating conductor layer [23]. The conductors in the reflector layer are essential for collecting and reflecting electromagnetic waves distributed in free space. The integrated reflector is also a thin-film attachment for cells having a composition of conductor and insulator and semi-conductor materials that optimizes the design structure of the integrated solar cell antenna.

2.1. Ring slot CP antenna structure configuration

The need for components to obtain high gain density then the antenna panel architecture is based on optimized radio frequency (RF) design, i.e., for electromagnetic energy harvesting, it is a more reliable power dissipation structure. The proposed dual-port antenna ring slot is configured to perform according to the International Telecommunication Union (ITU) standard allocation band for scientific and medical (ISM) bands for various radio telecommunications services as a complex electromagnetic environment (EM) infrastructure [24]. This band was chosen for RF energy harvesting and IoT communication and wireless sensor research with both functions active. Integrating a compact antenna with 4-layer components and two main microstrips with a thickness of 1.6 mm is an original work. This separation is necessary to preserve other electromagnetic structures critical to the operation of the receiving and transmitting system, such as IoT communications and wireless sensors [25], [26].

Figure 2 describes the configuration of a microstrip patch connected with a circular polarization aperture antenna. The antenna consists of two layers, with a reflector substrate of a white phenolic sheet rotating material ($\epsilon_r = 4.2$, $\tan = 0.0018$, $h = 0.0035$ mm) in which a ring slot with a two-port patch antenna is installed, and a 50 Ohm SubMiniature version A (SMA) port is used for network feeding. The finite element method (FEM) analysis method in the 3D high-frequency design software is used to optimize the implementation and design of the structure.

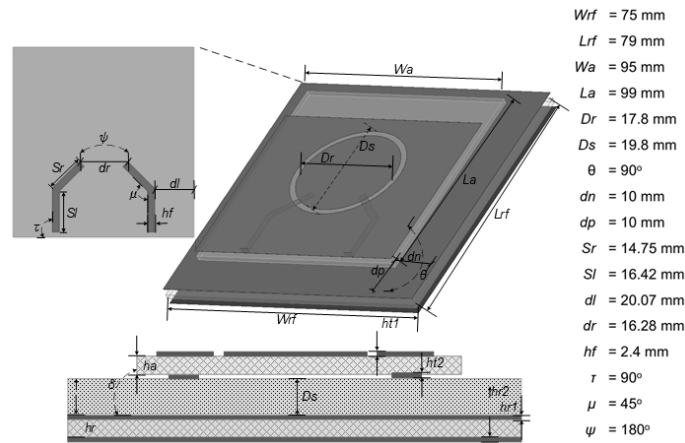


Figure 2. Implementation structure of a ring slot double-feed CP antenna

The patch antenna connected to the aperture was chosen as the best shape to reduce the feed tissue radiation that could disturb the primary pattern of the radiation area. Since the antenna ground plane separates the straight configuration between microstrip feed and circular strip and the slot is more narrow than the resonance size, the guaranteed radiation comes mainly from the patch element of resonant [27], [28]. Assuming the patch element of resonance is in its dominate mode, the approximate field in the cavity formed by the patch as the radiator and the magnetic wall around the periphery of its ring slot are expressed in (1).

$$f_{Rs} \approx \frac{c}{\pi(R_{Ds} + R_{DR})} \times \left(\frac{\epsilon_r + 1}{2\epsilon_r} \right)^{\frac{1}{2}} \quad (1)$$

The permittivity of the substrate FR4 is ϵ_r , where c is 3×10^8 m/s. The f_{rs} resonance frequency is 2.4 GHz, essentially the same as the resonant frequency with a lower axial ratio. The (1) is a rough formula for predicting the operating frequency of the two CP modes for the ring slot antennas examined, and they have apparent drawbacks if the slot width $R_{Ds} + R_{DR}$ is too thin or thick. The inaccuracy is less than 4% when the slot width is 0.002 m. It's better than [29].

The ring slot in the design has the advantage that most of them can independently adjust the resonance frequency of the CP antenna with a specific frequency range against other antenna parameters with the frequency shift in Figure 3. However, the dimensions of the ring slot must be symmetrical. On the entire surface at each change so that the resulting polarization remains circular [30]. Circular polarization is also adopted from the slot electromagnetic filter, in which electromagnetic waves propagate to the feed antenna and bounce of the reflector.

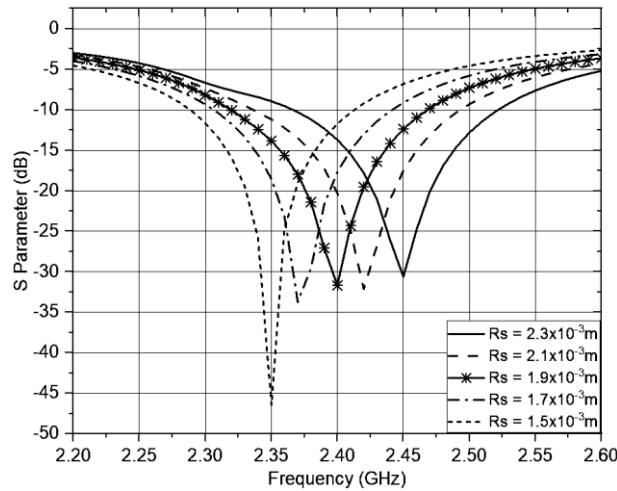


Figure 3. Tuning resonance frequency CP antenna

Frequency tuning with ring slot R_s variable based on the circular ground dimension is obtained from $R_s \approx R_{Ds} - R_{Dr}$. R_s value has an accuracy of changes up to 2×10^{-4} m at narrowband frequencies so that the frequency capture on the antenna design is following the implementation.

2.2. Hybrid electromagnetic solar doubler circuit design

The narrowband rectifier produced in the previous study was used in our investigation to rectify radio frequency or electromagnetic signals in the rectenna. It is the only suitable rectifier in the antenna in this study with an ideal 3-step voltage multiplier. However, the authors would like to point out that solar electromagnetic hybrids for energy harvesting using dual feed slot ring slots CP antennas can be applied to multiple channels rectenna in conjunction with IoT communication or wireless sensors. The narrowband rectifier is only used to demonstrate the harvesting capability of hybrid electromagnetic solar in principle. The keysight-advanced design system (ADS) schematic circuit of the rectifier used for the design is presented in Figure 4, a low barrier multi diode (SMS-761) in a multi-stage rectifier configured to work at a 2.4 GHz resonance frequency Table 1.

Table 1. Electronic components circuit of the hybrid electromagnetic solar

Elements	Discrete device	Material and parts
Semiconductor substrate	h	Phenolic sheet (FR-4) (1.6 mm)
Copper transmission conductor	hl2	Copper (0.035 mm)
Dimensions of the circuit	Lu, Wu	34.47 mm, 24.44 mm
SMD diode-multi-stage	D1-D19	SMS-761
Organic thin film solar cell	hl1	1 mm
SMD stage non-polar capacitor	C7, C5, C3, C1	100 uF - tantalum
	C6, C4, C2	10 nF - tantalum

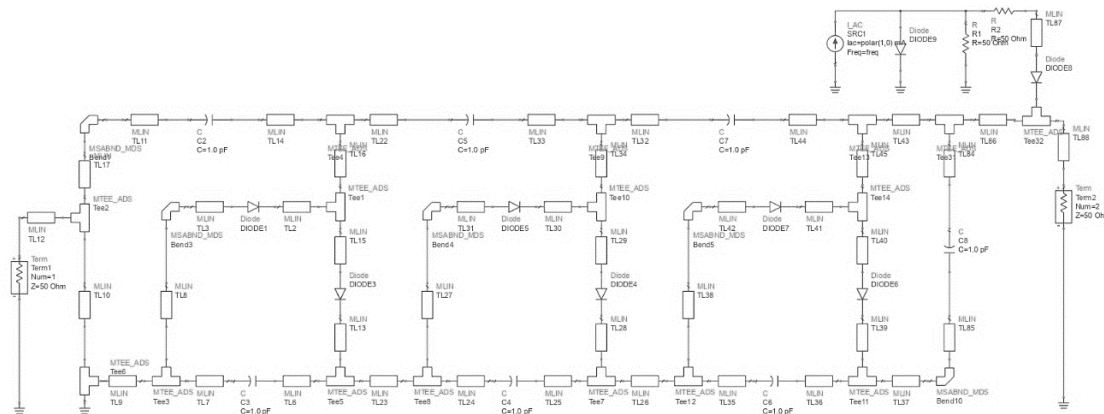


Figure 4. The schematic circuit design of hybrid electromagnetic solar

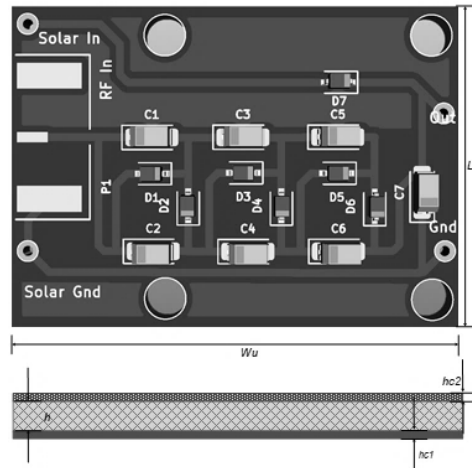


Figure 5. Configuration circuit implementation of hybrid electromagnetic solar

To improve the voltage circuit output's accuracy with specific components, so the optimization of inductance and capacitance of the configuration are also represented in the circuit configuration design in Figure 5, as shown in Table 1. The design voltage multiplier setting helps in increasing the voltage sensitivity [31]. The antenna's EM radiation is received by the rectifier circuit, which converts it to direct current (DC) power.

3. PERFORMANCE AND ANALYSIS

3.1. Double feed ring slot CP antenna

According to the following design, the ring slot antenna has a two-port CP mode with the same radiation pattern and polarization sensitivity. The available CP bandwidth is increased by effectively linking dual feeds with ring slot mode. The impedance matching optimization gets the value for the design feed in the same frequency range. According to the parametric analysis results on an L-shaped feed line, setting its dimensions in width and length to achieve the goal with width and length being used to adjust CP performance first. Then impedance matching is done by tuning the circular shape section. The prototype implementation of the structure is presented in Figure 6(a) and Figure 6(b).

This research measured the antenna using the measurement setup of a Rhode and Schwarz Z.V.L. 9 kHz to 13.6 GHz network analyzer. Figure 7 presents the CP Antenna S parameter measured. It can analyze that the antenna with dual feed ring slot has a balanced operating frequency band, and the resulting bandwidth in Figure 7 demonstrates a shift in frequency between $|S_{11}|$ and $|S_{22}|$. Measurement and range 100 MHz. Port-1 or $|S_{11}|$ under -15 dB has a range of resonance bands of 2.311–2.418 MHz (108 MHz), while $|S_{22}|$ or Port-2 under -15 dB has a range of resonance bands of 2.320–2.416 MHz (84 MHz).

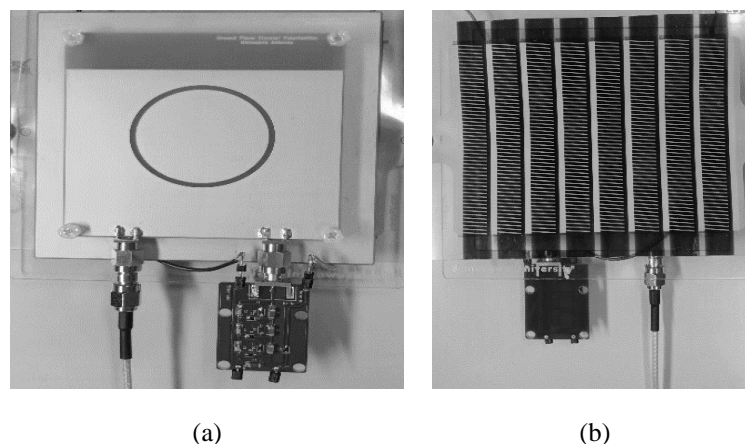


Figure 6. Compact implementation of double feed ring slot CP antenna for the hybrid electromagnetic solar energy harvesting and IoT application: (a) front and (b) rear

Figure 8 shows the power gain level and axial ratio performance of the ring slot CP Antenna. As observed from the figure, the axial ratio bandwidth is still below 3 dB. For linear polarized antennas reconfigured with CP polarization, the bandwidth overlap between the impedance bandwidth and the axial ratio bandwidth is usually used to evaluate the bandwidth characteristics of the CP antenna of 15%. And the gain level of the antenna has a high gain of 8.38 dB at 2.4 GHz. It is due to optimizing the reflector layer and integrating solar cells, which have a conducting material that can collect and distribute electromagnetic waves to the primary antenna.

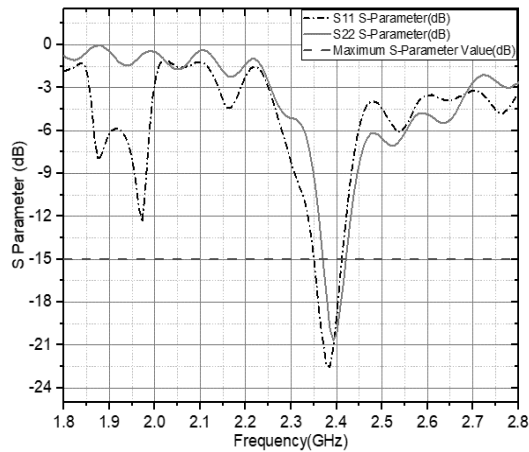


Figure 7. S-parameters of each port double feed ring slot CP antenna

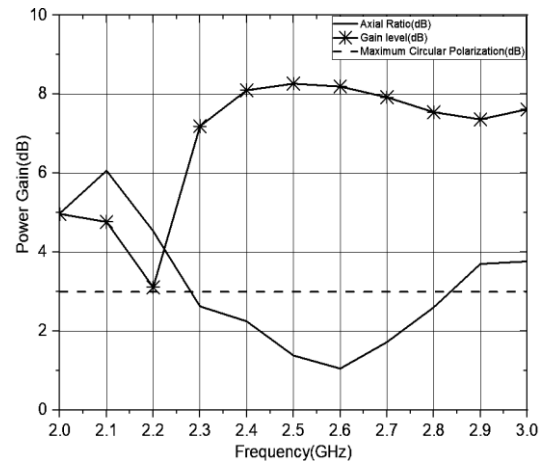


Figure 8. Gain level and axial ratio of each port double feed ring slot CP antenna

Performance, the radiation pattern in the *H* and *E* planes at an operating frequency of 2.4 GHz, is described in Figure 9, Figure 10(a) and Figure 10(b). The radiation pattern for the implementation to the *Z* coordinate axis looks directional with the maximum *Z* to the main lobe. So the antenna can implement for enabling inside and outside of the wireless sensors access at 8 dB gain range when a solar panel with an integrated antenna module is placed to a glass window or a glass structure. Of course, more effort is required to increase the gain even further to extend the transmission range.

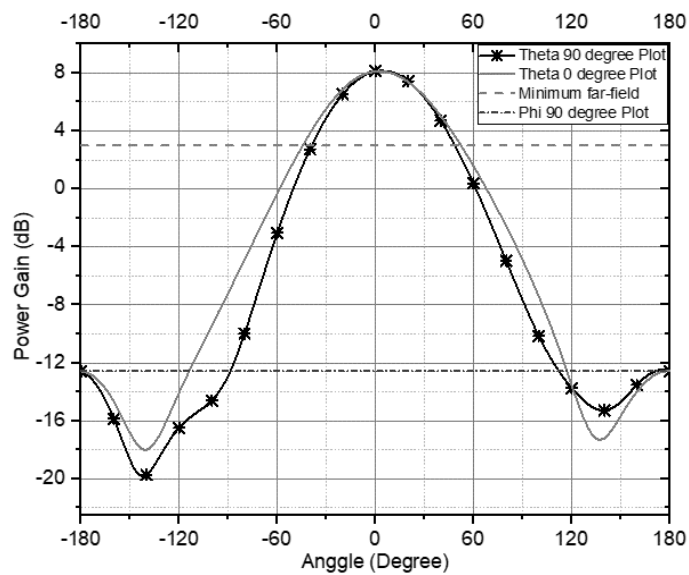


Figure 9. A rectangular plot of power level radiation pattern

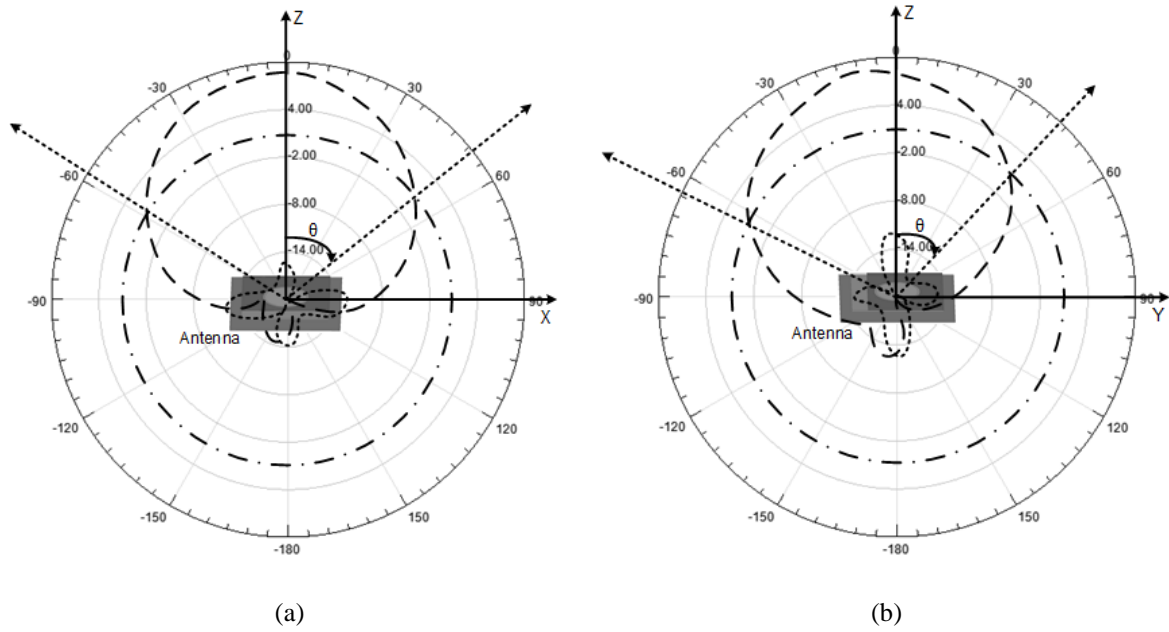


Figure 10. The plot of circular radiation pattern shape area: (a) θ angle and (b) Φ angle

3.2. Integrated the hybrid electromagnetic solar energy harvesting and IoT application

The performance evaluation of the integrated rectenna and solar cells was based on the measurement results. In the measurement process based on empirical RF distribution, the model in Figure 11 is adopted with the type of ISM antenna transmitter empirically used in the telecommunications industry, namely SHARP RZ1AT4A, which is carried out in the laboratory. By independently setting the transmission power of the generator signal simultaneously on the antenna, which is integrated with the electromagnetic harvesting system. It is crucial to describe the transmission power value of the spectrum level received by the antenna as a reference value of the resonance frequency of 2.4 GHz in Figure 12.

To test the received signal level performance, it is necessary to take a spectrum sample from electromagnetic wave transmission. The electromagnetic wave transmission spectrum level is calculated into five sample levels to represent the antenna working frequency at 2.4 GHz. With a spectrum transmission rate of 9.57 dBm, 0.27 dBm, -8.4 dbm, -16.8 dBm, and -31.32 dBm, the spectrum was adopted as a whole empirically the transmission of scattered electromagnetic waves.

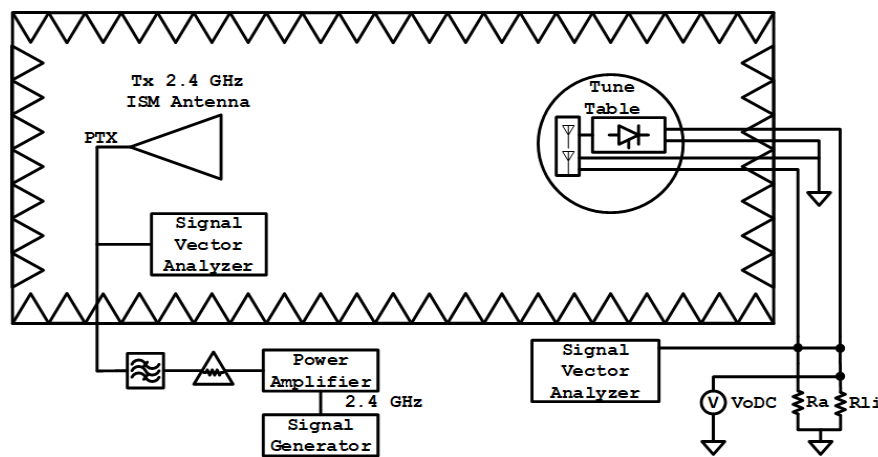


Figure 11. Performance test scheme of double feed ring slot CP antenna for the hybrid electromagnetic solar energy harvesting

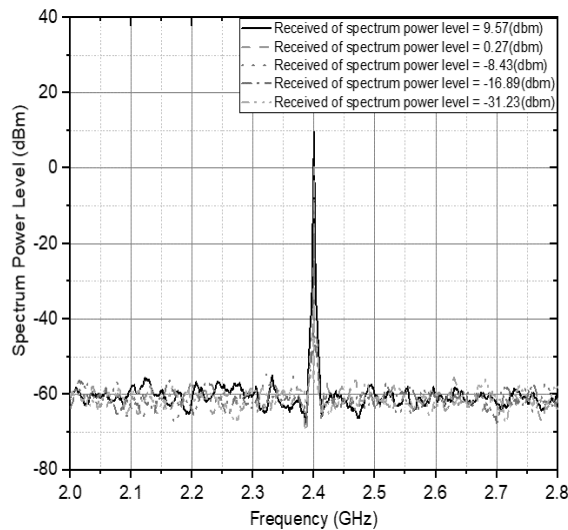


Figure 12. Spectrum power level received of double feed ring slot CP antenna

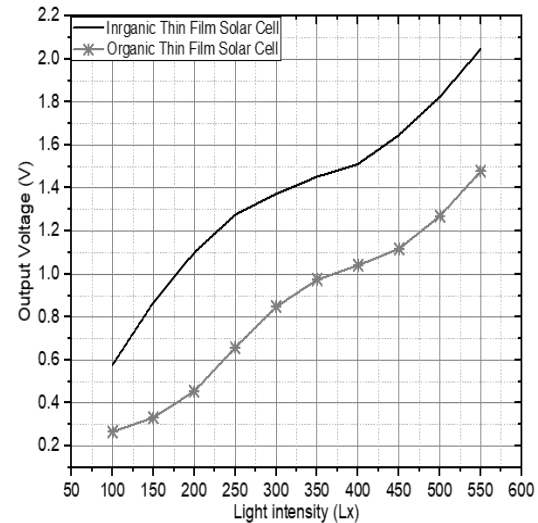


Figure 13. Conversion of optical energy into voltage output in organic and inorganic thin-film solar cells

To have sufficient light to stimulate organic thin-film solar cells in outdoor settings are combined by adopting a source of LED lamps with settings for the level of illumination. In Figure 13, we get the ability of thin-film solar with organic materials cells to convert optic energy into electrical energy DC. When compared to organic thin-film solar cells, the voltage generated by inorganic is higher. Still, if implemented with a communication circuit, this has a significant effect because the semi-conductor material as an acceptor layer in a $p - n$ junction can change the incoming or reflected waves on the integrated circuits. Therefore, the prototype implementation of this research uses organic thin-film solar cells. Finally, the entire integrated circuit is evaluated based on the DC voltage level collected through the RF and solar sources [17], [32]. By simultaneously comparing the two in Figure 5, it is obtained that the increase in energy harvesting using a tiny electromagnetic source with the optimization of solar sources can increase the DC voltage output level up to 20×. But the RF source is essential if the light source is unavailable, such as in dark conditions and low light luminance areas.

The power level captured by the antenna is 9.57 dBm, the spectrum level from the SHARP RZ1AT4A antenna as an RF source is obtained with a DC voltage of 33.7 mV at 2.4 GHz in Figure 14. The research optimization has been proven empirically with a significant increase in the experiment in Figure 15, so the series analysis is based on formula two. It proved to be better than [33], [34]. From the research results, the output voltage value can be analyzed based on a compactly built circuit using (2). The (2) represents the maximum voltage value. It is obtained when the final result of the integrated circuit integration has been optimized as an integrated electromagnetic energy harvester.

$$V_{PC} = \frac{\Delta n V_0}{n_0 R_a + R_{li}} R_{li} \quad (2)$$

The (2) represents an empirical performance-efficient circuit. The resistance value of the circuit is R_{li} , the voltage of DC output from the antenna integration with the voltage doubler is V_{PC} , and R_a is the medium transmission internal resistance. The coefficient of characteristic is n of the quantity of the doubler circuit with the optimization carried out by three doubler processes.

The analysis of the application of this energy harvesting circuit integration is intended to be applied empirically. Hence, the optical intensity carried out in the experiment is also based on the level of light luminance in the sun in general, namely 100 Lx – 2000 Lx. The lowest luminance value is when it is cloudy in the room, based on the performance test. It gives the lowest DC output, the circuit is still sensitive and works optimally to obtain DC energy. In addition to energy harvesting, it is simultaneously integrated with wireless sensor circuits in IoT communication with empirical conditions of multi-signal applications [35], [36]. Therefore, it is essential to analyze the signal propagation process by analyzing the classification model with multi-sample antennas with circular polarization sensitivity to obtain information on the number of signals and direction of multi signals arrival based on theta angle on the antenna radiation multi-patch element in Figure 16.

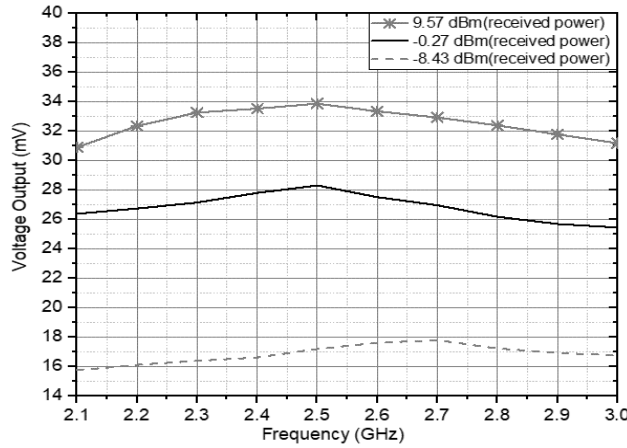


Figure 14. Comparison of circuit output voltage to frequency based on antenna received power level

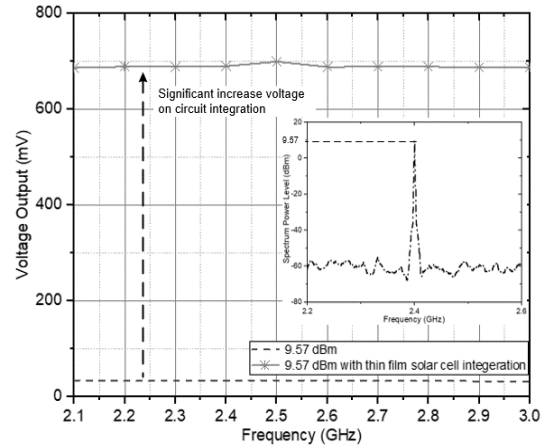


Figure 15. Increasing the output voltage level on the integration of organic thin-film solar cell circuit

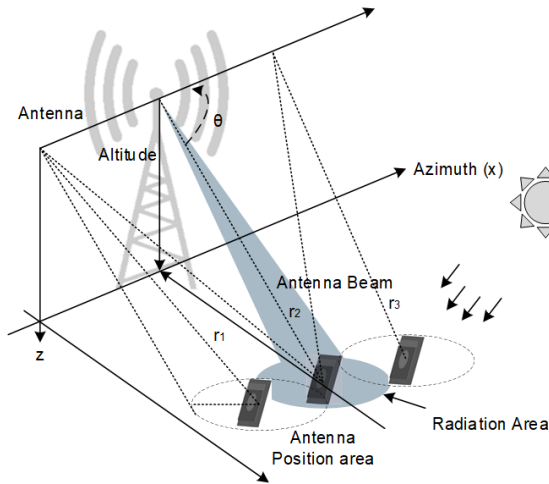


Figure 16. Analysis on overall implementation of an organic prototype thin-film solar cell with rectenna for integrated communications

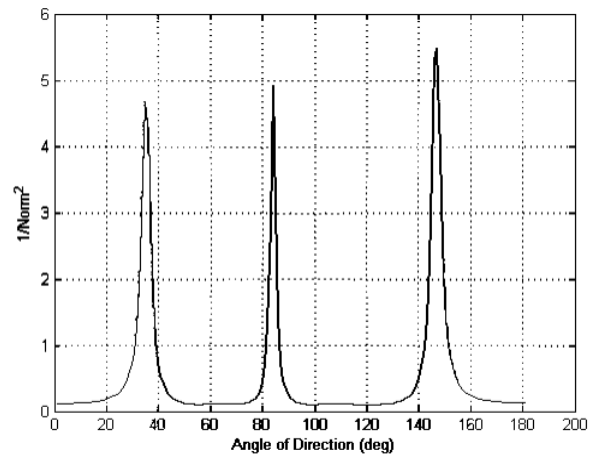


Figure 17. The multiple antennas spectrum analysis for incoming signals

In Figure 16, the analysis is completed by sending multiple sample signals of 1000 propagation times with three antennas with the azimuth position of Theta transmission. The steering vector of the incident wave value is α .

$$\alpha(\theta) = \begin{bmatrix} 1 \\ e^{j2\pi r_1 \sin\theta_1 / 1.25 \times 10^2} \\ e^{j2\pi r_2 \sin\theta_2 / 1.25 \times 10^2} \end{bmatrix} \tag{3}$$

The antenna coordinates on the azimuth axis, whose direction is perpendicular to the multi-patch antenna, represent the planar position, where r is the range between the device and the multi antennas of reference point and θ is the antenna transmission angle, as shown in Figure 16. The application of the wireless sensor device at a 2.4 GHz on the RF antenna signal with f is a variant amplitude [37]. Then it can be decomposed into (4) as $X(f)$.

$$\begin{bmatrix} X(f_1) \\ X(f_2) \\ X(f_3) \end{bmatrix} = [\alpha(\theta_1) \quad \alpha(\theta_2) \quad \alpha(\theta_3)] \begin{bmatrix} f_1 e^{j4.8 \times 10^9 \pi t} \\ f_2 e^{j4.8 \times 10^9 \pi t} \\ f_3 e^{j4.8 \times 10^9 \pi t} \end{bmatrix} \tag{4}$$

This matrix adds random amplitude to the covariance matrix of signal transmission from the source IoT device to the wireless sensor as \mathcal{S} in (5).

$$\mathcal{S} = \begin{bmatrix} -0.2577 - 4.0966i & -2.806 + 0.3545i & \dots & -1.5837 + 2.7315e - 13i \\ -0.0177 - 0.2814i & -0.7723 + 0.0975i & \dots & 0.0664 - 1.1453e - 14i \\ -0.0952 - 1.5131i & -0.9173 + 0.1158i & \dots & 0.6014 - 1.0373e - 13i \end{bmatrix} \quad (5)$$

The value between the input signal on the resultant steering vector $f e^{j4.8 \times 10^9 \pi t}$ and A is the steering matrix of $\alpha(\theta)$. The output data $\alpha(\theta)$ is $x = A \times \mathcal{S}$ dan x^* is the complex conjugate of the ensemble average, then we get $\overline{x_1 x_1^*}, \overline{x_2 x_2^*}, \overline{x_3 x_3^*}$ which is autocorrelated with R_{ss} [38], [39]. The input signal is then autocorrelated, the signal's other cross-correlation values assume the signal plane, and the input signal's matrix covariance is calculated in (6) and (7).

$$x = \begin{bmatrix} -0.52723 - 8.3316i & -6.3732 + 0.8032i & 0.5832 + 3.0702i & 1.8096 - 0.4615i \\ 6.3143 - 2.4699i & -1.8207 - 3.3461i & 1.9521 - 0.7679i & -2.0575 - 6.0008i \\ 2.3535 + 4.9307i & 4.2190 - 1.5907i & \ddots & -3.9329 - 1.2190i \\ -3.2380 + 0.7227i & 0.8750 + 1.5609i & \dots & 1.9233 - 1.2135i \end{bmatrix} \quad (6)$$

$$\overline{xx^*} = \begin{bmatrix} \overline{x_1 x_1^*} & \overline{x_1 x_2^*} & \overline{x_1 x_3^*} \\ \overline{x_2 x_1^*} & \overline{x_2 x_2^*} & \overline{x_2 x_3^*} \\ \overline{x_3 x_1^*} & \overline{x_3 x_2^*} & \overline{x_3 x_3^*} \end{bmatrix} = A R_{ss} A^* + P_{noise} \quad (7)$$

Then, define the noise power eigenvector and $A R_{ss} A^*$ eigenvector. It extracts information and generates the signal eigenvalue and noise eigenvalue with the noise subspace value by defining the noise subspace with matrix D in the matrix in (8) [37].

$$D = \begin{bmatrix} 8.5083e - 05 & 0 & 0 & 0 \\ 0 & 8.9625e - 05 & 0 & 0 \\ 0 & 0 & \ddots & 0 \\ 0 & 0 & \dots & 61.9601 \end{bmatrix} \approx \begin{bmatrix} 1 & 0 & 0 & 0 \\ 0 & 1 & 0 & 0 \\ 0 & 0 & \ddots & 0 \\ 0 & 0 & \dots & 1 \end{bmatrix} \quad (8)$$

From each value of information and noise, define the level of the signal reservoir by describing each order on the eigen noise = e_i and signal eigenvalues with the equation $(\sum_{i=F-1}^M |e_i^* \alpha(\theta)|^2)^{-1}$. From this process, you can use the classification equation for several signals in the equation to obtain a spectral image of each signal $(\alpha^*(\theta) \cdot e_i \cdot e_i^* \cdot \alpha(\theta))^{-1}$.

The spectrum results analysis can be partially expressed as the origin signal angle and the incoming signal information, although the phase is nearly identical to the random amplitude condition. The origin angle of the proximity signal to one another in the antenna area is described in Figure 17. The spectrum performs the signal originating from the CP antenna with the angle direction of arrival. Based on the level value of the normalized power level $1/\text{Norm}^2$ on every signal. For the sample of analysis, the data indicates at 35, 85, and 145 degrees. Therefore, this analysis can be an efficient solution for IoT communication between the wireless sensor antenna and the energy receiver in the proposed prototype implementation using a closed site antenna with a circular polarization sensitivity antenna specification.

4. CONCLUSION

In this research, IoT communication devices that utilize electromagnetic waves have been developed to harvest electromagnetic energy and solar energy simultaneously, have sensitivity to vertical and horizontal waves, and accommodate so that cross-polarization does not occur with the CP antenna. The circularly polarized antenna configuration circuit has a dual feed ring slot with 84 MHz two-port bandwidth under -15 dB and less than 3 dB axial ratio with 8.38 dB gain at 2.4 GHz center frequency. Optimization by developing a compact primary antenna integrated with a solar panel layer and a rectifier circuit to produce a voltage power level for IoT connectivity and low-power energy harvesting has a maximum radiation value of 9.57 dBm from a transmitter with a voltage of 685 mV with the organic thin-film solar cells integration in a prototype and a compact composition on hold. With circuit analysis and multiple signal classification on signals for communication on wireless sensors, IoT devices can work well and have compact configurations and optimal energy harvesting rates. It is necessary to develop the circuit to add a phase shifter to the passive circuit connected to the antenna and then apply it to the analysis of multi-signal classification with the adaptive structure of the antenna.




REFERENCES

- [1] W. An, L. Hong, Y. Luo, K. Ma, J. Ma, and X. Huang, "A Wideband Dual-Function Solar Cell Dipole Antenna for Both Energy Harvesting and Wireless Communications," *IEEE Transactions on Antennas and Propagation*, vol. 69, no. 1, pp. 544-549, 2021, doi: 10.1109/TAP.2020.3005250.
- [2] F. Erkmen and O. M. Ramahi, "A Scalable, Dual-Polarized Absorber Surface for Electromagnetic Energy Harvesting and Wireless Power Transfer," *IEEE Transactions on Microwave Theory and Techniques*, vol. 69, no. 9, pp. 4021-4028, 2021, doi: 10.1109/TMTT.2021.3087622.
- [3] B. Xi, X. Liang, Q. Chen, K. Wang, J. Geng, and R. Jin, "Optical Transparent Antenna Array Integrated with Solar Cell," *IEEE Antennas and Wireless Propagation Letters*, vol. 19, no. 3, pp. 457-461, 2020, doi: 10.1109/LAWP.2020.2969694.
- [4] W. An, L. Xiong, S. Xu, F. Yang, H. -P. Fu, and J. -G. Ma, "A Ka-Band High-Efficiency Transparent Reflectarray Antenna Integrated With Solar Cells," *IEEE Access*, vol. 6, pp. 60843-60851, 2018, doi: 10.1109/ACCESS.2018.2875359.
- [5] F. Meddour, H. Bencherif, A. Boukarkar, M. A. Abdi, and M. Amir, "An efficient hybrid solar and electromagnetic harvesting system for autonomous operation of small sensors," *Optik*, vol. 208, 2020, doi: 10.1016/j.ijleo.2019.164022.
- [6] D. A. Prasetya and I. Mujahidin, "2.4 GHz Double Loop Antenna with Hybrid Branch-Line 90-Degree Coupler for Widespread Wireless Sensor," in *2020 10th Electrical Power, Electronics, Communications, Controls and Informatics Seminar (EECCIS)*, 2020, pp. 298-302, doi: 10.1109/EECCIS49483.2020.9263477.
- [7] C. Bahhar, C. Baccouche, and H. Sakli, "Optical Rectenna for Energy Harvesting and RF Transmission in Connected Vehicles," in *2020 17th International Multi-Conference on Systems, Signals & Devices (SSD)*, 2020, pp. 262-266, doi: 10.1109/SSD49366.2020.9364243.
- [8] H. Kim, W. Choe, and J. Jeong, "A terahertz CMOS V-shaped patch antenna with defected ground structure," *Sensors*, vol. 18, no. 8, 2018, doi: 10.3390/s18082432.
- [9] A. Rashidian, L. Shafai, and C. Shafai, "Miniaturized Transparent Metalodielectric Resonator Antennas Integrated with Amorphous Silicon Solar Cells," *IEEE Transactions on Antennas and Propagation*, vol. 65, no. 5, pp. 2265-2275, 2017, doi: 10.1109/TAP.2017.2679492.
- [10] M. Wagih, A. S. Weddell, and S. Beeby, "Powering E-Textiles Using a Single Thread Radio Frequency Energy Harvesting Rectenna," *Proceedings*, vol. 68, no. 1, 2021, doi: 10.3390/proceedings2021068016.
- [11] J. -M. L. -Garde, R. D. -R. -Ruiz, J. Legarda, and H. Rogier, "2 × 2 textile rectenna array with electromagnetically coupled microstrip patch antennas in the 2.4 GHz WiFi band," *Electronics*, vol. 10, no. 12, 2021, doi: 10.3390/electronics10121447.
- [12] S. Muhammad, J. J. Tiang, S. K. Wong, A. Smida, R. Ghayoula, and A. Iqbal, "A dual-band ambient energy harvesting rectenna design for wireless power communications," *IEEE Access*, vol. 9, pp. 99944-99953, 2021, doi: 10.1109/ACCESS.2021.3096834.
- [13] T. A. Elwi, "Electromagnetic band gap structures based on ultra wideband microstrip antenna," *Microwave and Optical Technology Letters*, vol. 59, no. 4, pp. 827-834, 2017, doi: 10.1002/mop.30397.
- [14] F. M. A. Hamied, K. R. Mahmoud, M. Hussein, and S. S. A. Obayya, "Design and analysis of hexagonal dipole nano-rectenna based on MIIM diode for solar energy harvesting," in *2020 8th International Japan-Africa Conference on Electronics, Communications, and Computations (JAC-ECC)*, 2020, pp. 100-103, doi: 10.1109/JAC-ECC51597.2020.9355947.
- [15] S. X. Ta, J. J. Lee, and I. Park, "Solar-Cell Metasurface-Integrated Circularly Polarized Antenna with 100% Insolation," in *IEEE Antennas and Wireless Propagation Letters*, vol. 16, pp. 2675-2678, 2017, doi: 10.1109/LAWP.2017.2740570.
- [16] Q. Chen, Z. Li, W. Wang, Z. Huang, X. Liang, and X. Wu, "A Broadband Dual-polarized Solar Cell Phased Array Antenna," *IEEE Transactions on Antennas and Propagation*, vol. 70, no. 1, pp. 353-364, 2022, doi: 10.1109/TAP.2021.3098520.
- [17] O. O'Conchubhair, P. McEvoy, and M. J. Ammann, "Dye-sensitized solar cell antenna," *IEEE Antennas and Wireless Propagation Letters*, vol. 16, pp. 352-355, 2017, doi: 10.1109/LAWP.2016.2576687.
- [18] M. Elsdon, O. Yurduseven, and X. Dai, "Wideband metamaterial solar cell antenna for 5 GHz WiFi communication," *Progress in Electromagnetics Research C*, vol. 71, pp. 123-131, 2017, doi: 10.2528/PIERC16110302.
- [19] J. Zhang, N. Li, Z. Sun, and Q. Yi, "Structural design of a bow-tie nano-rectenna for solar energy collection," in *Lecture Notes in Electrical Engineering*, 2020, vol. 588, doi: 10.1007/978-981-32-9437-0_87.
- [20] A. I. Imran, T. A. Elwi, and A. J. Salim, "On the distortionless of uwb wearable hilbert-shaped metamaterial antenna for low energy applications," *Progress In Electromagnetics Research M*, vol. 101, pp. 219-239, 2021, doi: 10.2528/PIERM20113008.
- [21] I. Mujahidin and A. Kitagawa, "The Novel CPW 2 . 4 GHz Antenna with Parallel Hybrid Electromagnetic Solar for IoT Energy Harvesting and Wireless Sensors," *International Journal of Advanced Computer Science and Applications*, vol. 12, no. 8, pp. 393-400, 2021. [Online]. Available: https://thesai.org/Downloads/Volume12No8/Paper_45-The_Novel_CPW_2.4_GHz_Antenna_with_Parallel_Hybrid.pdf
- [22] T. R. Jones, J. P. Grey, and M. Daneshmand, "Solar panel integrated circular polarized aperture-coupled patch antenna for cubesat applications," *IEEE Antennas and Wireless Propagation Letters*, vol. 17, no. 10, pp. 1895-1899, 2018, doi: 10.1109/LAWP.2018.2869321.
- [23] S. S. Panigrahi, G. P. Mishra, and B. B. Mangaraj, "Antenna Array Beam Scanning and SINR Visualization on a Map for 5G Urban Macro-Cell Test Environment," in *2020 International Conference on Wireless Communications Signal Processing and Networking (WiSPNET)*, 2020, pp. 107-111, doi: 10.1109/WiSPNET48689.2020.9198568.
- [24] I. Mujahidin and A. Kitagawa, "The Compact 2.4 GHz Hybrid Electromagnetic Solar Energy Harvesting (HES-EH) circuit using Seven Stage Voltage Doubler and Organic Thin Film Solar Cell," in *2021 4th International Seminar on Research of Information Technology and Intelligent Systems (ISRITI)*, 2021, pp. 640-645, doi: 10.1109/ISRITI54043.2021.9702844.
- [25] U. Pattapu and S. Das, "Capacitive coupled circular patch antenna based rectenna systems for 5.8 GHz wireless power transfer applications," *International Journal of RF and Microwave Computer-Aided Engineering*, vol. 31, no. 7, 2021, doi: 10.1002/mmce.22675.
- [26] O. M. Dardeer, H. A. Elsadek, E. A. Abdallah, and H. M. Elhennawy, "A dual band circularly polarized rectenna for RF energy harvesting applications," *The Applied Computational Electromagnetics Society Journal (ACES)*, vol. 34, no. 10, 2019. [Online]. Available: <https://journals.riverpublishers.com/index.php/ACES/article/view/8185>
- [27] C. A. Balanis, *Antenna Theory: Analysis and Design*, Fourth Edition, John Wiley Sons, Inc., 2016. [Online]. Available: <https://www.wiley.com/en-us/Antenna+Theory%3A+Analysis+and+Design%2C+4th+Edition-p-9781118642061>
- [28] I. Mujahidin, D. A. Prasetya, Nachrowie, S. A. Sena, and P. S. Arinda, "Performance tuning of spade card antenna using mean average loss of backpropagation neural network," *International Journal of Advanced Computer Science and Applications (IJACSA)*, vol. 11, no. 2, 2020, doi: 10.14569/ijacsa.2020.0110280.
- [29] Y. Han, L. Zhu, Y. Bo, W. Che, and B. Li, "Novel Low-RCS Circularly Polarized Antenna Arrays via Frequency-Selective Absorber," *IEEE Transactions on Antennas and Propagation*, vol. 68, no. 1, pp. 287-296, 2020, doi: 10.1109/TAP.2019.2939845.
- [30] A. Quddious, S. Zahid, F. A. Tahir, M. A. Antoniadis, P. Vryonides, and S. Nikolaou, "Dual-Band Compact Rectenna for UHF and ISM Wireless Power Transfer Systems," *IEEE Transactions on Antennas and Propagation*, vol. 69, no. 4, pp. 2392-2397,




- 2021, doi: 10.1109/TAP.2020.3025299.
- [31] M. Muhibbullah, A. A. Alhazime, A. M. A. Haleem, and S. E. El-Zohary, "Theoretical and experimental investigations on optimization of the received power of a monopole antenna," *Physica Scripta*, vol. 96, no. 1, 2021, doi: 10.1088/1402-4896/abc509.
- [32] N. D. Au, H. Le-Huu, and C. Seo, "A Wide Dynamic-Range Rectifier at 433 MHz for Multiple-Antenna Impedances," *IEEE Microwave and Wireless Components Letters*, vol. 31, no. 2, pp. 196-199, 2021, doi: 10.1109/LMWC.2020.3036375.
- [33] P. Prakasam, T. R. S. Kumar, T. Velmurugan, and S. Nandakumar, "Efficient power distribution model for IoT nodes driven by energy harvested from low power ambient RF signal," *Microelectronics Journal*, vol. 95, 2020, doi: 10.1016/j.mejo.2019.104665.
- [34] Y. Luo, J. Lai, N. Yan, W. An, and K. Ma, "Integration of Aperture-Coupled Multipoint Feed Patch Antenna with Solar Cells Operating at Dual Compressed High-Order Modes," *IEEE Antennas and Wireless Propagation Letters*, vol. 20, no. 8, pp. 1468-1472, 2021, doi: 10.1109/LAWP.2021.3087500.
- [35] F. Zhang, C. Wu, B. Wang, and K. J. R. Liu, "MmEye: Super-Resolution Millimeter Wave Imaging," *IEEE Internet of Things Journal*, vol. 8, no. 8, pp. 6995-7008, 2021, doi: 10.1109/JIOT.2020.3037836.
- [36] R. Kawdungta, S. Kawdungta, D. Torrungrueng, and C. Phongcharoenpanich, "Switched Beam Multi-Element Circular Array Antenna Schemes for 2D Single-Anchor Indoor Positioning Applications," *IEEE Access*, vol. 9, pp. 58882-58892, 2021, doi: 10.1109/ACCESS.2021.3072951.
- [37] V. Dakulagi, "A new approach to achieve a trade-off between direction-of-arrival estimation performance and computational complexity," *IEEE Communications Letters*, vol. 25, no. 4, pp. 1183-1186, 2021, doi: 10.1109/LCOMM.2020.3048023.
- [38] A. M. Ahmed, U. S. K. P. M. Thantrige, A. El Gamal, and A. Sezgin, "Deep Learning for DOA Estimation in MIMO Radar Systems via Emulation of Large Antenna Arrays," *IEEE Communications Letters*, vol. 25, no. 5, pp. 1559-1563, 2021, doi: 10.1109/LCOMM.2021.3053114.
- [39] I. Mujahidin and A. Kitagawa, "CP Antenna with 2×4 Hybrid Coupler for Wireless Sensing and Hybrid RF Solar Energy Harvesting," *Sensors*, vol. 21, no. 22, 2021, doi: 10.3390/s21227721.

BIOGRAPHIES OF AUTHORS



Irfan Mujahidin    he is a Ph.D. student in Electrical Engineering and Computer Science, Kanazawa University, Japan. He was born in East Java, Indonesia, in 1992. He received a Bachelor of Engineering in Electrical Engineering from the Brawijaya University, Malang, Indonesia, in 2015 and a Master of Science in Institute of Communication Engineering, National Sun Yat-sen University, Kaohsiung, Taiwan, the Republic of China in 2018. His current research interests include antenna design on RF energy harvesting, wireless sensor networks, Internet-of-Things applications, wireless power transmission, and RF circuit design. He can be contacted at email: irfan@merl.jp.



Akio Kitagawa    was born in Hikone, Japan in 1961. He received the BE, the ME, and the Ph.D. degree from Nagoya Institute of Technology, Nagoya, Japan, in 1985, 1987, and 1991, respectively. Since 1989, he has worked for the Department of Electrical and Computer Engineering, Kanazawa University, Japan. From 1997 to 1998, he went abroad to study in Microsystems Technology Laboratories (MTL), Massachusetts Institute of Technology (MIT), USA. Since 1999 I transferred to VLSI Design and Education Center (VDEC), The University of Tokyo, Japan. From 2001 to 2003, he was with the Department of Information and Systems Engineering, Kanazawa University, Japan. From 2004 to 2007, he had been with the Division of Electrical Engineering and Computer Science, Graduate School of Natural Science and Technology, Kanazawa University. Since 2008 he works with the College of Science and Engineering, School of Electrical, Information and Communication Engineering at Kanazawa University. His research interests include phase change nonvolatile RAM, VLSI design automation, Integrated Sensor Systems, RF circuit design, and VLSI applications to mobile systems. He can be contacted at email: kitagawa@is.t.kanazawa-u.ac.jp.